Investigation of Thin AlBGaN Layers Grown by MOVPE

Oliver Rettig

In this article, epitaxial growth of AlBGaN layers and superlattices with boron content in the lower percentage regime are investigated. The focus of this work lies on the growth development of thin layers and their luminescent properties. Only very few reports in literature investigate photoluminescence of these layers due to the poorer crystal quality compared to conventional AlGaN layers. Here we show that the addition of boron to AlGaN leads to 3D-like growth with tilted facets. In contrast to thicker layers, thin layers of AlBGaN layers show similarly strong luminescence compared to AlGaN layers, and therefore have potential for applications in UV-LEDs.

1. Introduction

Group III nitrides such as InN, GaN, AlN and their alloys have attracted a lot of interest due to their potential in providing high efficiency electronic and optoelectronic devices in a broad spectral regime including UV-C through to the whole visible spectrum [1]. Whereas for InGaN based blue to green LEDs already very high efficiencies have been achieved, AlGaN based UV devices still suffer from relatively poor external quantum efficiencies below 21 % [2]. Over the recent years a lot of progress has been made to reduce problems like high dislocation densities in AlGaN epitaxial layers [3], low carrier injection efficiency into the active region [3] and low light outcoupling efficiency [2]. Another major challenge is the very strong internal field in the quantum well (QW) active region due to lattice mismatch, leading to a strong decrease in overlap of the carrier wave functions and thus to a decrease in internal quantum efficiency. As a potential material allowing to reduce the strain in the QW, AlBGaN has been proposed [4]. By adding boron as the lightest and smallest group III element to the currently used AlGaN system, another degree of freedom in band gap and lattice constant tailoring can be utilized. To lattice-match AlBGaN QWs with an aluminium content of 50 % to an AlN barrier, a boron incorporation below 6 % would be sufficient [5, 6]. However, the solubility of boron in AlGaN is very low.

Recent experimental studies show single phase epitaxial growth of AlBN for boron contents up to ∼10 % [7]. However, provided TEM micrographs seem to indicate irregularities in the crystalline structure which might be due to the fact that the solubility limit is reached if not even exceeded, as evidenced by spinodal isotherm calculations where a maximum boron content of 3 % for a stable phase in AlN and GaN is predicted for a growth temperature of 1000 °C [8, 9]. This may be also the reason that up to now we could not find acceptable photoluminescence data of AlBGaN layers even with low B content in the open literature.

Considering state-of-the-art UV-LED devices [2], $Al_xGa_{1-x}N$ quantum wells ($x = 0.4$) and barriers ($x = 0.55$) have a difference in aluminium composition of $\Delta x = 15\,\%$. Lattice matching of both layers could be achieved by incorporating only small B amounts of about 2 % in the quantum wells, assuming the validity of Vegard's law and lattice constants of 0.3112 nm, 0.3189 nm, and 0.2549 nm for the binaries AlN, GaN, and wurtzite BN, respectively [6, 10]. Still, the low solubility, but also parasitic gas phase reactions and low surface mobility of boron, make it very challenging to grow high quality quaternary AlBGaN alloys with appropriate optoelectronic properties [11,12,14]. In this research, we therefore concentrate on the MOVPE growth and characterization of AlBN and AlBGaN layers with low B content. We try to retain good crystallinity for boron containing layers with good luminescence characteristics to study the applicability of this quaternary material in future LEDs.

2. Experimental Details

For this study a low-pressure horizontal flow MOVPE reactor (Aixtron Aix-200/4 RF-S) with high-temperature kit is used, allowing growth temperatures up to 1400 °C. For all experiments 500–900 nm thick AlN templates were used which were grown on (0001) sapphire substrates with a 0.3° offcut towards the m-plane. The optimized AlN templates show a full width at half maximum (FWHM) below 50 arcsec and 1000 arcsec for the (0002) and $(10\bar{1}2)$ reflexes, respectively, in high resolution x-ray diffraction (HRXRD). Precursors for epitaxial growth were trimethyl-aluminium (TMAl), trimethyl-gallium (TMGa), triethyl-boron (TEB), and ammonia (NH_3). Ex-situ characterization involves, besides HRXRD, aberration-corrected high-resolution transmission electron microscopy (AC-HRTEM), low temperature photoluminescence spectroscopy (PL) at 8 K with an argon fluoride excimer laser excitation source ($\lambda = 193$ nm), atomic force microscopy (AFM) and secondary ion mass spectrometry (SIMS). For cross-sectional TEM investigations, the samples were ground to a thickness of 100 µm and further trenched down below 5 µm. Ion milling was performed with 5 kV at 10° incident angle in a Fischione Ion Mill 1010. Liquid nitrogen cooling was applied to reduce amorphization due to ion bombardment.

3. Results and Discussion

3.1 Growth of thin AlBGaN layers

The results presented above indicate that thin layers with low B content may have good crystalline properties. To further investigate the development of 3D growth and its impact on the PL characteristics of the layers, thin single AlBGaN layers were grown on AlN templates. Ga was added to the thin layers to be able to clearly identify luminescence from the boron containing layer besides the luminescence of the AlN template. The B/III-ratio was chosen to be 0.7 % due to the trend for better crystal quality at lower boron contents [14]. Further, the Ga/III-ratio was set to 46 %, the reactor pressure was set to 35 hPa and the surface temperature is kept at 1160 °C. On similarly grown single layer structures, SIMS measurements revealed a boron and Ga incorporation of ∼1 % and

∼30 %, respectively. This leads to an estimated lattice mismatch between the AlBGaN and AlN layers of ∼0.5 %. Corresponding AFM studies of layers with thicknesses from 5–20 nm are displayed in Fig. 1.

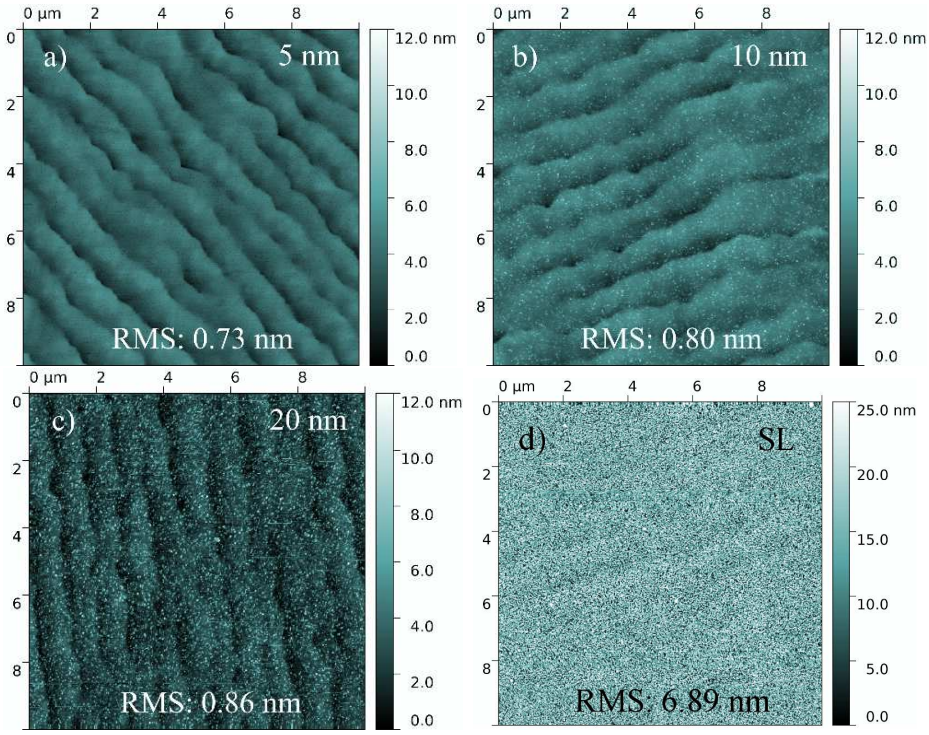

Fig. 1: AFM images (10 µm × 10 µm) of AlBGaN layers with varying thicknesses (a–c) and from an AlBGaN/AlN superlattice structure (d).

Growth steps, visible in all AFM images, originate from the AlN template. Even after 20 nm of AlBGaN growth, they are still visible, indicating an ongoing 2D growth mode not heavily impacted by the presence of boron. Also the RMS roughness values of the surface do not significantly increase when comparing 5 nm and 20 nm thick layers with values of 0.73 nm and 0.86 nm, respectively, showing that the growth is mainly occurring in 2D mode.

Table 1: Comparison of the dislocation and grain densities of the investigated samples.

Sample	template disloc. density	column/grain
300 nm AlBN	$<10^{10}\,\mathrm{cm}^{-2}$	$\sim 2 \cdot 10^{11}\,\mathrm{cm}^{-2}$
10 nm AlBGaN	$<10^{10}\,\mathrm{cm}^{-2}$	$\sim 1.6 \cdot 10^{9}\,\mathrm{cm}^{-2}$
20 nm AlBGaN	$<10^{10}\,\mathrm{cm}^{-2}$	$\sim 1.2 \cdot 10^{10}\,\mathrm{cm}^{-2}$

However, small grainy features can be observed on the surfaces starting from 10 nm thick AlBGaN layers. This is exemplarily shown in Fig. 2, exhibiting a magnified part of the sample of Fig. 1 (b). The features become more pronounced and their density increases from $\sim 1.6 \cdot 10^{9}\,\mathrm{cm}^{-2}$ for a 10 nm thick AlBGaN layer to $\sim 1.2 \cdot 10^{10}\,\mathrm{cm}^{-2}$ for a 20 nm thick layer. The densities are calculated by counting the white spots present in the 10 µm × 10 µm AFM micrographs (Fig. 1), which have heights typically around 2–3 nm,

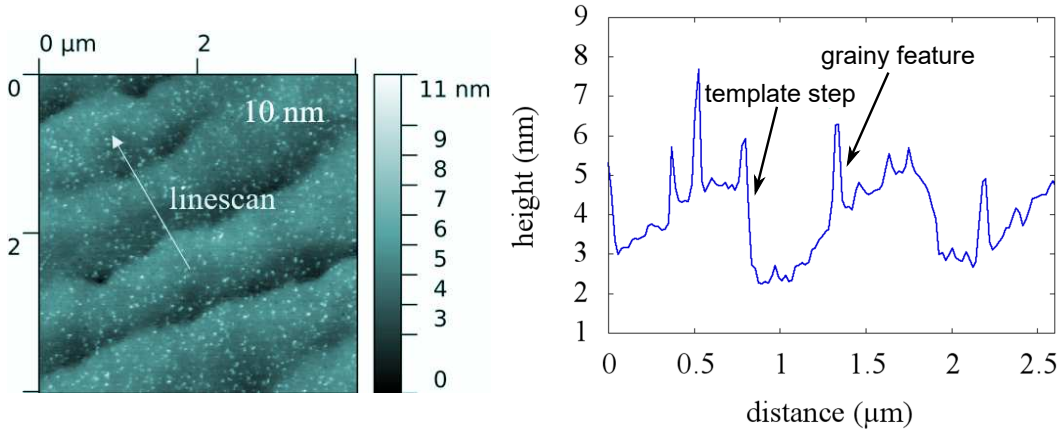

Fig. 2: AFM line profile (right) of the 10 nm thick AlBGaN layer measured perpendicular to the steps on the template (left).

as illustrated in a line scan in Fig. 2. They have an average width of ∼30 nm, which is in good agreement with the width of the columns observed for our thicker AlBN layers [13] and columnar sizes found by Li et al. [14,15]. The density of the columns ($\sim 2 \cdot 10^{11}\,\mathrm{cm}^{-2}$) measured on the samples shown in the previous annual report [13] exceeds the density of the threading dislocations ($<10^{10}\,\mathrm{cm}^{-2}$) estimated from XRD calculations by over an order of magnitude (see also Table 1). Therefore, we exclude a correlation between columnar growth or the formation of grains and the threading dislocation density. Also no evidence of such a dependence was found in weak-beam dark-field investigations on similar samples.

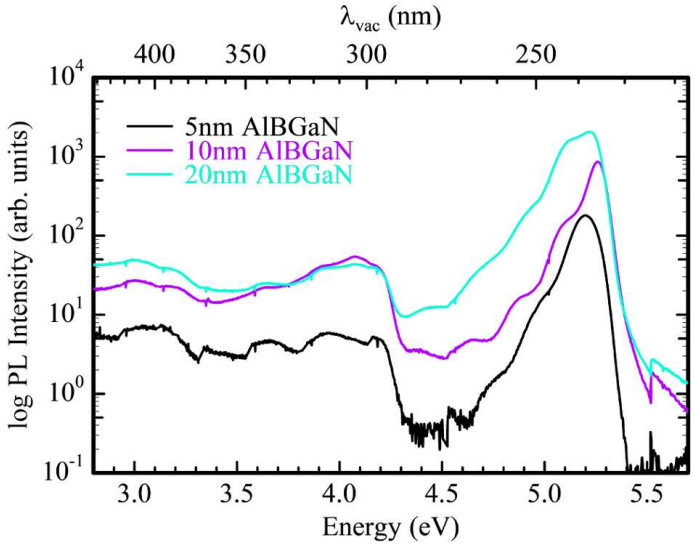

Fig. 3: PL spectra from an AlBGaN layer thickness series from 5–20 nm.

Logarithmic PL spectra from the thin layers are displayed in Fig. 3. The peak at 5.2 eV can be attributed to the near band edge (NBE) luminescence of AlBGaN. The dependence of the band edge energy and the composition in AlBN or BGaN is not yet well known.

Theoretical calculations for wurtzite BN predict a direct and indirect band gap of 10.2 eV and 6.8 eV, respectively [16]. For the bowing parameters of the direct band gap of AlBN high values of ∼7 eV can be approximated from graphs shown by Zhang et al. [16]. BGaN also exhibits strong bowing of ∼3.61 eV [17]. Hence for 1 % of boron in AlN and GaN, only small shifts of the band gap energy in the range of −20 meV to −40 meV are expected. Therefore, the band gap energy is predominantly defined by the AlGaN composition.

From the NBE luminescence at 5.2 eV it is clearly visible that layers up to 20 nm thickness containing about ∼1 % of boron maintain good luminescence yields despite the presence of small 3D growth features. In these spectra, the NBE luminescence intensity increases for thicker layers, showing no sign of deterioration of the crystal quality. This might be partially due to the fact that the optically active volume increases for thicker layers. In the energy range 4.5–5.2 eV, Fabry–Pérot fringes are visible, which correlate with the thickness of the template (∼900 nm). The broadening of the NBE peak might be caused by compositional fluctuations of the thin AlBGaN layers.

We attribute the broad band ranging from 3 eV [18, 19] to 4 eV [19–21] to silicon, oxygen and carbon related defects and their complexes. Their intensities are not strongly influenced by the layer thickness, despite the roughening of the surface which could have indicated a deterioration of the crystal quality and increase in structural defects.

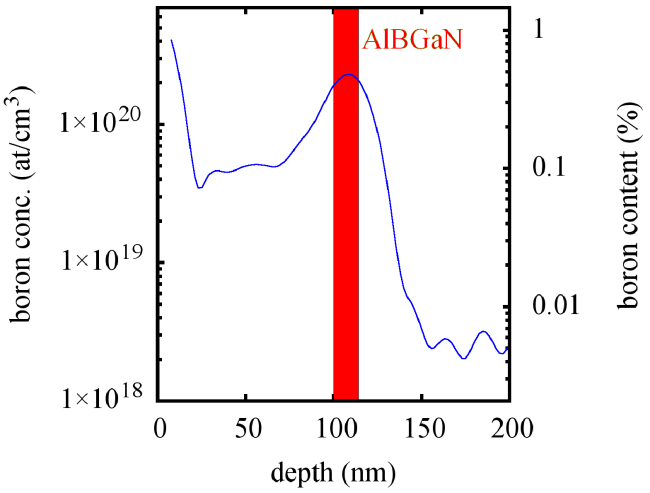

Fig. 4: SIMS measurement of the boron concentration of a ∼14 nm thick AlBGaN layer capped by 100 nm of AlN.

For thicker boron containing layers, columnar growth was observed [13]. The change in growth mode from 2D to a 3D process might have influence on the boron incorporation efficiency into Al(Ga)N. Therefore, SIMS investigations were performed on thin layers. For this study an additional sample was grown under the same growth conditions as described above. Due to artefacts at the start of the SIMS measurement, which can be observed in the concentration profile at the surface (Fig. 4), the thin AlBGaN layer needs to be buried in a capping layer, in this case chosen to be 100 nm AlN. The thickness of the AlBGaN layer is ∼14 nm. However, the boron signal smears over a depth more than that. This is attributed to the already depicted roughness of AlN capped AlBGaN, which

reduces the depth resolution in SIMS. Therefore, the boron concentration was evaluated by integrating the total amount of boron divided by the initial AlBGaN layer thickness. This results in a boron content of ∼1.5 %. However, the actual boron content in AlBGaN might be slightly lower in case of a memory effect of boron in the gas phase. After the decrease of the B concentration curve, between about 75 and 25 nm SIMS depth, the B signal levels off at a significantly higher level than the AlN template's background noise level of boron ($\sim 2 \cdot 10^{18}\,\mathrm{cm}^{-3}$ at 150 nm and deeper). This could be an indication of a memory effect of boron.

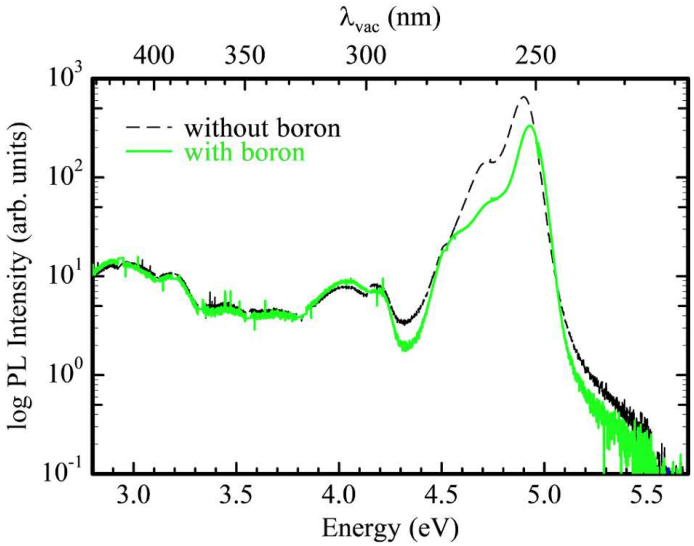

Fig. 5: Low temperature PL spectra at 7 K from an AlBGaN and an AlGaN layer with a thickness of 20 nm each, grown on the same template only differing in an extra supply of TEB.

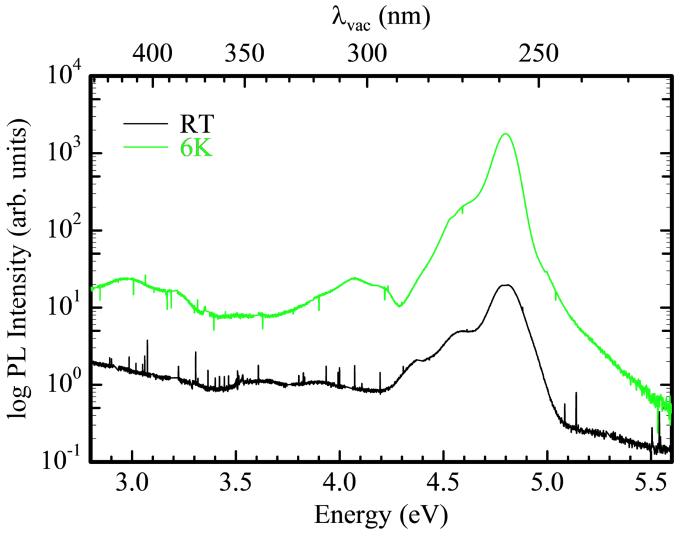

Fig. 6: Room and low temperature PL spectra from a 20 nm thick AlBGaN layer.

A direct comparison of the PL of B-containing and B-free layers grown otherwise under

the same conditions is depicted in Fig. 5. Compared to the samples shown in Fig. 3, these samples have slightly increased Ga supply in the gas phase from 46 % to 54 %, which results in a redshift. As described above, with the incorporation of small amounts of boron, a negative energy shift of the NBE luminescence is expected. However, in Fig. 5 a minor positive change of the peak energy of ∼30 meV is observed. Again, small Al/Ga composition shifts from run to run or across the sample area may cause such differences. The B-containing layer shows quite strong PL with about half the intensity of the boron-free layer. Both layers show a broadening of the NBE peak towards lower energies. This might be attributed to composition fluctuations in the AlGaN or AlBGaN layers. No enhanced defect luminescence between 3 eV and 4 eV is visible (Fig. 5) for the boron containing layer as compared to pure AlGaN layers. This indicates, that the presence of boron does not promote the formation of silicon, oxygen or carbon related vacancies. Therefore, we attribute the decrease in PL intensity to non-radiative recombination, presumably related to an increased amount of stacking faults and edge-type dislocations, as discussed in the next section.

A comparison of the room and low temperature PL spectra of an AlBGaN layer is shown in Fig. 6. We observe a strong decrease of about two orders of magnitude in band edge luminescence for the higher temperature. This is again an indication of a considerable amount of defects present in boron containing layers. No redshift can be observed for the room temperature PL compared to the measurement at 6 K, which would be expected due to the temperature dependence of the band gap. This might be explained by a local fluctuation of the Ga, Al and B compositions. At higher temperatures carriers also recombine at regions with locally higher Al content and consequently higher band gap energy, mitigating the reduction of the band gap at higher temperatures.

3.2 Growth of AlBGaN/AlN superlattice structure

To visualize the temporal development of the 3D growth, we grew an AlBGaN/AlN superlattice (SL) structure with thicknesses of approximately 7 nm and 10 nm, respectively, as confirmed by cross-section high angle annular dark field (HAADF)-STEM micrographs (Fig. 8). The growth conditions were kept the same as in the previous experiment. Hence the B content of the AlBGaN layers is estimated to be about 1 %.

Owing to the high amount of Ga in these layers, we observe very clear interfaces between the AlN and AlBGaN layers. As expected from the AlBN layers described in the previous annual report [13] and the thin AlBGaN layers in Sect. 3.1, the first AlBGaN/AlN interfaces are very smooth. However, in the upper AlBGaN layers a blurred contrast can be seen. After few periods, some 3D growth develops. The layer stacking still can be identified, but inclined facets occur for many areas in the cross-section, which may be explained by the formation of many small V-pit-like defects or more stable tilted side facets compared to c-plane. The blurring may be explained by the finite thickness of the TEM specimen, which is ∼100 nm, estimated from energy-filtered transmission electron microscopy (EFTEM) measurements. Hence we see a projection over randomly positioned V-pits. Due to the small thickness of the AlBGaN layers and the surface roughness, estimation of the boron content by HRXRD was not possible.

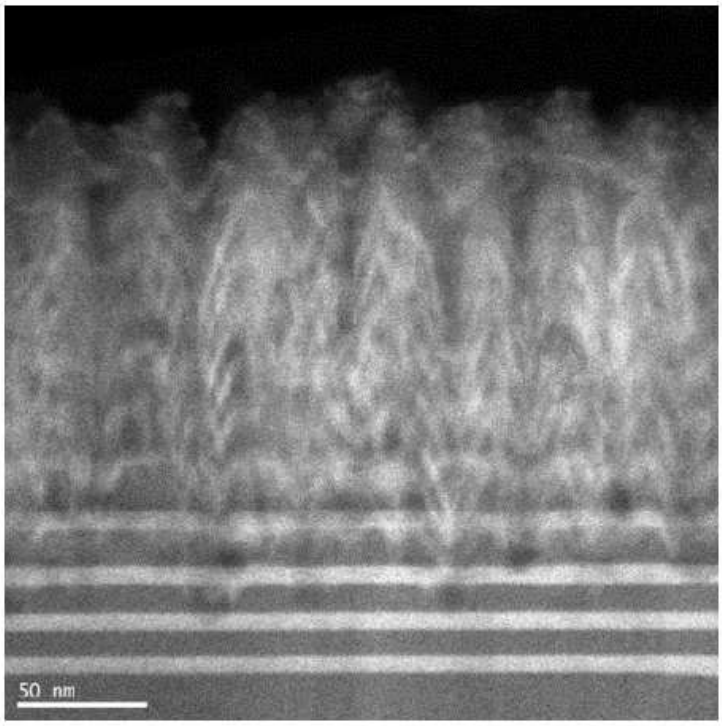

Fig. 7: HAADF image of an AlBGaN/AlN superlattice structure. The AlBGaN layers appear brighter than the AlN. The first periods grow nicely aligned, however, after a few stacks strong 3D growth can be observed.

Recent studies have shown that B-III-N based crystals can exhibit lattice twinning [22] or tilting [7]. SAED measurements (Fig. 8 a–d) were carried out to prove the absence of lattice twinning and polycrystalline growth. There are no additional diffraction spots apart from the wurtzite AlN in the lower SL region (Fig. 8 a,b). Here, the AlN template, the first well aligned SL periods and the upper part of the SL contribute to the diffraction pattern. Also investigations from only the upper part of the SL (Fig. 8 c,d) clearly show single phase wurtzite material without lattice twinning or tilting. The tilted facets visible in cross-section micrographs (Fig. 7) are therefore not occurring due to a tilt of the lattice planes, but refer to 3D growth with inclined facets. WBDF images from this sample show no correlation of threading dislocations and the columns. In Fig. 8 e) a cross-section image with Burgers vector $g = (0002)$ is displayed, making visible screw and mixed type threading dislocations. They already thread through the AlN template and continue through the first SL periods. After a few nanometers, the contrast changes indicating that these later grown layers exhibit a high amount of defects.

The fast Fourier transform (FFT) filtered HRTEM micrograph in Fig. 9 taken from the upper part of the AlBGaN SL confirms the c-direction alignment of the lattice also visible in selective area electron diffraction investigation.

It is again evident that the sharp tilted AlBGaN/AlN interfaces in the upper part of the SL stack are not originating from a tilting of lattice planes [11] but are caused by

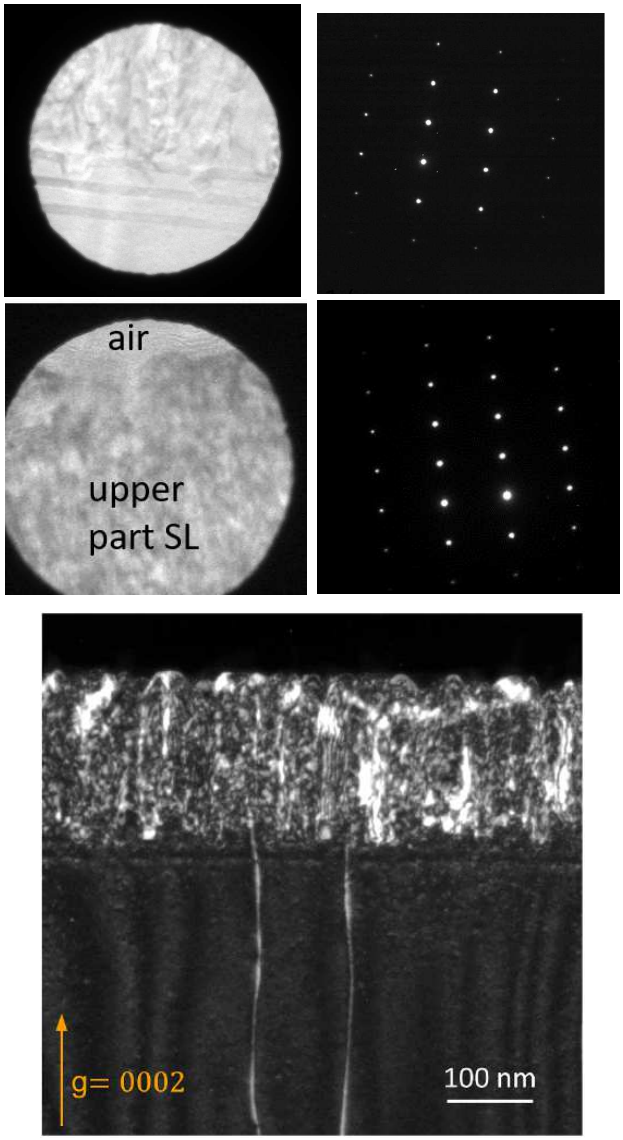

Fig. 8: SAED of the lower (top 2 images) and the upper (middle 2 images) part of the SL stack and WBDF (bottom image) investigation on the growth of the AlBGaN/AlN SL.

formation of tilted facets with higher Miller indices during growth. Additionally, many inserted half-planes can be seen in the micrograph, forming edge-type dislocations with Burgers vector in (0002) direction and propagation in the a-direction. Above those defects, planes are slightly bent to compensate for the mismatch caused by underlying defects. The vertical line defects illustrated in Fig. 9 (b) correspond to stacking faults, which are terminated by partial defects [15]. We do not attribute these defects to the occurrence of columnar-like growth, because their distance is much smaller than the observed column size [13]. Possibly more favourable tilted facets observed in the superlattice structure in Fig. 8 lead to the formation of grains and 3D growth.

These investigations show that by the superlattice approach overgrowing thin layers of AlBGaN by 10 nm of AlN, 3D growth can not be prevented. However, in this sample no

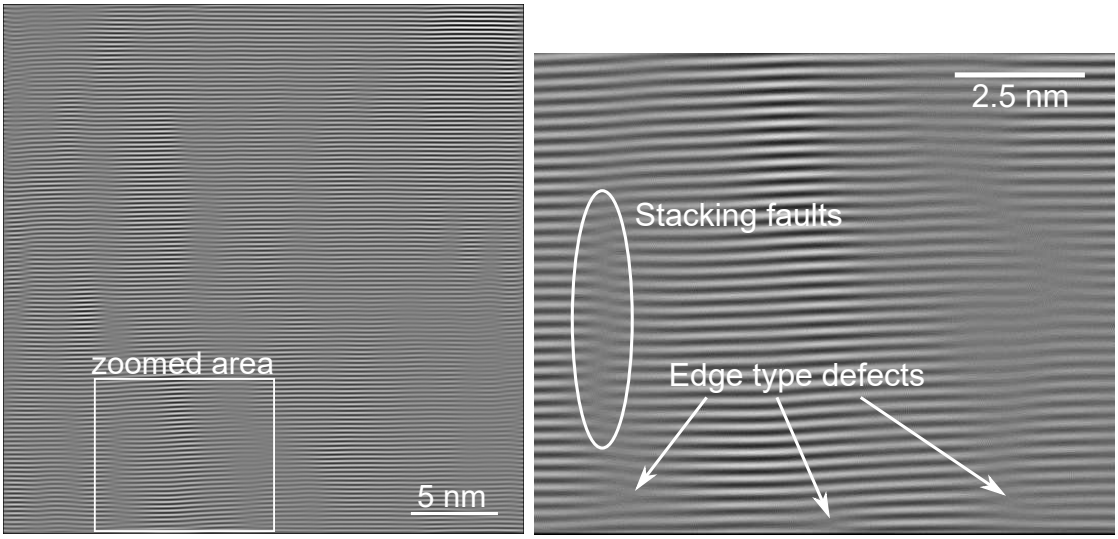

Fig. 9: FFT filtered HRTEM image (left) and therein indicated zoomed area (right) of the upper part (upper 20 nm) of the AlBGaN/AlN superlattice structure. Some planes end, forming horizontal edge-type dislocations. Vertical defect lines correspond to stacking faults with partial dislocations at their ends.

phase separation with formation of amorphous regions was found in TEM. This is possibly related to the decrease in boron content leading to better crystalline quality. Additionally, growing only 7 nm of B-containing material followed by 10 nm of AlN and the presence of Ga might delay the appearance of amorphous phases.

4. Conclusion

For the growth of AlBN and AlBGaN layers, we have observed the development of 3D growth. No correlation between the density of the grains and the threading dislocation density could be seen. Even when separating thin B containing layers by pure AlN, 3D growth is observed after a few superlattice periods, which results in inclined facets. For the growth of thin AlBGaN layers from 5–20 nm, good PL yields were observed with no sign of degradation. Also smooth layers with predominantly 2D growth behaviour were observed in AFM measurements. However, small grain-like features develop starting from thicknesses of 10 nm. Their density is increasing with thickness, and their size matches the diameter of the columns previously observed for AlBN. Since no degradation of the PL intensity occurs, these 3D features do not seem to strongly affect the crystalline quality. For optimized growth conditions, AlBGaN layers show a PL peak intensity about half of that of corresponding B-free AlGaN layer.

Acknowledgment

I thank the coauthors N. Steiger, J.-P. Scholz, S. Bauer, M. Hocker, and K. Thonke of the Institute of Quantum Matter, Semiconductor Physics Group at Ulm University for

optical characterization and help with AFM, XRD and CL spectroscopy, Y. Li, H. Qi, J. Biskupek, and U. Kaiser of the Central Facility of Electron Microscopy at Ulm University for performing TEM analysis, and T. Hubáček and M. Zíková of the Institute of Physics, Czech Academy of Sciences, Prague, Czech Republic for their scientific support with epitaxy, AFM and XRD. This work is financially supported by the Deutsche Forschungsgemeinschaft (DFG). We thank Probion Analysis (Bagneux, France) for the SIMS investigations.

References

[1] S.O. Kasap and P. Capper (Eds.), *Springer Handbook of Electronic and Photonic Materials*, New York: Springer, 2006.

[2] T. Takano, T. Mino, J. Sakai, N. Noguchi, K. Tsubaki, and H. Hirayama, "Deep-ultraviolet light-emitting diodes with external quantum efficiency higher than 20 % at 275 nm achieved by improving light-extraction efficiency", *Appl. Phys. Express*, vol. 10, pp. 031002-1–4, 2017.

[3] M. Kneissl, T. Kolbe, C. Chua, V. Kueller, N. Lobo, J. Stellmach, A. Knauer, H. Rodriguez, S. Einfeldt, Z. Yang, N.M. Johnson, and M. Weyers, "Advances in group III-nitride-based deep UV light-emitting diode technology", *Semicond. Sci. Technol.*, vol. 26, pp. 014036-1–6, 2011.

[4] S. Sakai, Y. Ueta, and Y. Terauchi, "Band gap energy and band lineup of III-V alloy semiconductors incorporating nitrogen and boron", *Jpn. J. Appl. Phys.*, vol. 32, pp. 4413–4417, 1993.

[5] K. Shimada, T. Sota, and K. Suzuki, "First-principles study on electronic and elastic properties of BN, AlN, and GaN", *J. Appl. Phys.*, vol. 84, pp. 4951–4958, 1998.

[6] A. Nagakubo, H. Ogi, H. Sumiya, K. Kusakabe, and M. Hirao, "Elastic constants of cubic and wurtzite boron nitrides", *Appl. Phys. Lett.*, vol. 102, pp. 241909-1–5, 2013.

[7] X. Li, S. Wang, H. Liu, F.A. Ponce, T. Detchprohm, and R.D. Dupuis, "100-nm thick single-phase wurtzite BAlN films with boron contents over 10 %", *Phys. Status Solidi B*, vol. 254, pp. 1600699-1–5, 2017.

[8] C.H. Wei and J.H. Edgar, "Unstable composition region in the wurtzite $B_{1-x-y}Ga_x Al_yN$ system", *J. Cryst. Growth*, vol. 208, pp. 179–182, 2000.

[9] T. Kimura and T. Matsuoka, "Calculation of phase separation in wurtzite $In_{1-x-y-z} Ga_xAl_yB_zN$", *Jpn. J. Appl. Phys.*, vol. 46, pp. L574–L576, 2007.

[10] M.A. Moram and M.E. Vickers, "X-ray diffraction of III-nitrides", *Reports on Progress in Physics*, vol. 72, pp. 036502-1–40, 2009.

[11] T. Akasaka and T. Makimoto, "Flow-rate modulation epitaxy of wurtzite AlBN", *Appl. Phys. Lett.*, vol. 88, pp. 041902-1–3, 2006.

[12] A.Y. Polyakov, M. Shin, W. Qian, M. Skowronski, D.W. Greve, and R.G. Wilson, "Growth of AlBN solid solutions by organometallic vapor-phase epitaxy", *J. Appl. Phys.*, vol. 81, pp. 1715–1719, 1997.

[13] O. Rettig, "Investigation of AlBN Grown by MOVPE", *Annual Report 2016*, pp. 59–66, Ulm University, Institute of Optoelectronics.

[14] X. Li, S. Sundaram, Y. El Gmili, T. Moudakir, F. Genty, S. Bouchoule, G. Patriarche, R.D. Dupuis, P.L. Voss, J.P. Salvestrini, and A. Ougazzaden, "BAlN thin layers for deep UV applications", *Phys. Status Solidi A*, vol. 212, pp. 745–750, 2015.

[15] Y. Li, H. Qi, T. Meisch, M. Hocker, K. Thonke, F. Scholz, and U. Kaiser, "Formation of I_2-type basal-plane stacking faults in $In_{0.25}Ga_{0.75}N$ multiple quantum wells grown on a (101-1) semipolar GaN template", *Appl. Phys. Lett.*, vol. 110, pp. 022105-1–4, 2017.

[16] M. Zhang and X. Li, "Structural and electronic properties of wurtzite $B_xAl_{1-x}N$ from first-principles calculations: structural and electronic properties of wurtzite $B_xAl_{1-x}N$", *Phys. Status Solidi B*, vol. 254, pp. 1600749-1–8, 2017.

[17] A. Said, M. Debbichi, and M. Said, "Theoretical study of electronic and optical properties of BN, GaN and $B_xGa_{1-x}N$ in zinc blende and wurtzite structures", *Optik – International Journal for Light and Electron Optics*, vol. 127, pp. 9212–9221, 2016.

[18] B.E. Gaddy, Z. Bryan, I. Bryan, J. Xie, R. Dalmau, B. Moody, Y. Kumagai, T. Nagashima, Y. Kubota, T. Kinoshita, A. Koukitu, R. Kirste, Z. Sitar, R. Collazo, and D.L. Irving, "The role of the carbon-silicon complex in eliminating deep ultraviolet absorption in AlN", *Appl. Phys. Lett.*, vol. 104, pp. 202106-1–4, 2014.

[19] K.B. Nam, M.L. Nakarmi, J.Y. Lin, and H.X. Jiang, "Deep impurity transitions involving cation vacancies and complexes in AlGaN alloys", *Appl. Phys. Lett.*, vol. 86, pp. 222108-1–3, 2005.

[20] P. Kamyczek, E. Placzek-Popko, V. Kolkovsky, S. Grzanka, and R. Czernecki, "A deep acceptor defect responsible for the yellow luminescence in GaN and AlGaN", *J. Appl. Phys.*, vol. 111, pp. 113105-1–7, 2012.

[21] S.F. Chichibu, H. Miyake, Y. Ishikawa, M. Tashiro, T. Ohtomo, K. Furusawa, K. Hazu, K. Hiramatsu, and A. Uedono, "Impacts of Si-doping and resultant cation vacancy formation on the luminescence dynamics for the near-band-edge emission of $Al_{0.6}Ga_{0.4}N$ films grown on AlN templates by metalorganic vapor phase epitaxy", *J. Appl. Phys.*, vol. 113, pp. 213506-1–6, 2013.

[22] S. Wang, X. Li, A.M. Fischer, T. Detchprohm, R.D. Dupuis, and F.A. Ponce, "Crystal structure and composition of BAlN thin films: effect of boron concentration in the gas flow", *J. Cryst. Growth*, vol. 475, pp. 334–340, 2017.